DOI: 10.1002/chem.200800881

Lanthanum Nitride Endohedral Fullerenes $La_3N@C_{2n}$ ($43 \leq n \leq 55$): Preferential Formation of $La_3N@C_{96}$

Manuel N. Chaur,[a] Frederic Melin,[a] Jarryd Ashby,[a] Bevan Elliott,[a] Amar Kumbhar,[b] Apparao M. Rao,[c] and Luis Echegoyen*[a]

Abstract: While the trimetallic nitrides of Sc, Y and the lanthanides between Gd and Lu preferentially template C_{80} cages, $M_3N@C_{80}$, and while those of Ce, Pr and Nd preferentially template the C_{88} cage, $M_3N@C_{88}$, we show herein that the largest metallic nitride cluster, La_3N, preferentially leads to the formation of $La_3N@C_{96}$ and to a lesser extent the $La_3N@C_{88}$. This is the first time that La_3N is successfully encapsulated inside fullerene cages. $La_3N@C_{2n}$ metallofullerenes were synthesized by arcing packed graphite rods in a modified Krätschmer–Huffman arc reactor, extracted from the collected soot and identified by mass spectroscopy. They were isolated and purified by high performance liquid chromatography (HPLC). Different arcing conditions were studied to maximize fullerene production, and results showed that yields have a high La_2O_3/C dependence. Relatively high yields were obtained when a 1:5 ratio was used. Three main fractions, $La_3N@C_{88}$, $La_3N@C_{92}$, and $La_3N@C_{96}$, were characterized by UV/Vis-NIR and cyclic voltammetry. Unlike other trimetallic nitride metallofullerenes of the same carbon cage size, $La_3N@C_{88}$ exhibits a higher HOMO–LUMO gap and irreversible reduction and oxidation steps.

Keywords: absorption · electrochemistry · fullerenes · HOMO–LUMO gaps · metallofullerenes

Introduction

Ever since Dorn and co-workers reported the synthesis of the first trimetallic nitride endohedral metallofullerene[1] in 1999 these compounds have attracted a great deal of interest due to their electronic and structural features. They are known to be nondissociative salts, where the metallic nitride cluster donates six electrons to the carbon cage with the general formula $M_3N^{6+}@C_{2n}{}^{6-}$.[2]

Metallic nitride endohedral fullerenes have been synthesized mainly by two methods: the trimetallic nitride template method proposed by Dorn,[1] where packed graphite rods (metal oxide/carbon/catalyst) are burned in the presence of a dynamic flow of He/N_2, and the reactive-gas atmosphere method introduced by Dunsch,[3] where the packed graphite rods (metal oxide/graphite) are burned in the presence of He/NH_3. The most attractive feature of these synthetic methods is that metallic clusters with highly paramagnetic and electroactive metals can be encapsulated inside fullerene cages making them potential candidates for numerous applications in different fields.[4,5]

As of today, fullerene encapsulation of several metallic nitrides have been reported, including group III metals (Sc and Y), lanthanides (Lu, Yb, Tm, Er, Ho, Dy, Tb, Gd, Nd, Pr and Ce), and mixed metal clusters.[1,3,6–13] For some time it was believed that metallic nitride clusters larger than Gd_3N could not be encapsulated inside fullerene cages for three reasons: 1) the known pyramidalization of this metallic cluster inside the C_{80} cage, 2) the fact that fullerene yield decreases dramatically from Sc to Gd, and 3) trimetallic nitride endohedral metallofullerenes of larger metals like Eu and Sm had not been successfully produced.

However, we recently reported that metals larger than Gd can form metallic nitride endohedral fullerenes,[14,15] and that these metallic clusters are preferentially encapsulated inside the C_{88} cage. It seemed that the metallic cluster induced the formation of a new carbon cage size around it

[a] M. N. Chaur, Dr. F. Melin, J. Ashby, B. Elliott, Prof. Dr. L. Echegoyen
Chemistry Department, Clemson University
219 Hunter Laboratories
Clemson, SC 29630-0973 (USA)
Fax: (+1) 864-656-6613
E-mail: luis@clemson.edu

[b] A. Kumbhar
Advance Materials Research Laboratories, 91 Technology Dr.
Anderson, SC 29625 (USA)

[c] Prof. Dr. A. M. Rao
Department of Physics and Astronomy, Clemson University
Clemson, SC 29634 (USA)

that promoted the electronic stabilization between the encapsulated moiety and the cage, similar to the one for metallic nitride clusters (from Sc to Gd) and the C_{80} cage.[2] Thus, as the metallic cluster size increases, a new templating effect appears.[15] This statement was supported by the fact that from Nd to Ce the yield of $M_3N@C_{96}$ increases significantly although $M_3N@C_{88}$ predominates. This feature raised the question whether or not larger clusters such as La_3N would be preferentially encapsulated inside C_{96} cages.

Due to the large ionic radius of lanthanum in the metallic nitride cluster, $La_3N@C_{2n}$ metallofullerenes appear in very low yield, which makes the preparation of enough material for their characterization hard and time consuming. This has prevented researchers from studying this family of cluster fullerenes until now.

One of the most interesting features of metallic nitride endohedral fullerenes is their redox properties. $M_3N@C_{80}$ metallofullerenes exhibit similar trends in redox behavior. As the size of the carbon cage increases, increasingly reversible reduction steps are observed, until C_{88} where total reversibility is reached.[15,16] For instance, all $M_3N@C_{88}$ metallofullerenes feature two reversible reductions and oxidations with very low HOMO–LUMO gaps (around 1.4–1.5 V). So far, this reversible behavior is not well understood, but several electrochemical/ESR, as well as computational studies, have suggested that oxidation occurs in the carbon cage and reduction on the metallic cluster.[2,14–17] To the best of our knowledge, electrochemical studies for metallic nitride endohedral fullerenes with cages larger than C_{88} have never been reported.

Herein, we report the synthesis, isolation and characterization of the $La_3N@C_{2n}$ $(43 \leq n \leq 55)$ family. Three main fractions were characterized by matrix-assisted laser desorption/ionization time-of-flight (MALDI-TOF) mass spectrometry, HPLC, SEM/EDS, UV/Vis-NIR and cyclic voltammetry. Results indicate that La_3N constitutes the largest metallic cluster encapsulated in a fullerene cage, and that $La_3N@C_{92}$ and $La_3N@C_{96}$ represent the largest metallic nitride endohedral fullerenes isolated and characterized so far.

Results and Discussion

Synthesis of $La_3N@C_{2n}$ $(43 \leq n \leq 55)$ endohedral fullerenes: The synthesis of $La_3N@C_{2n}$ metallofullerenes was accomplished by using the reactive gas atmosphere method. Graphite rods were packed with different La_2O_3/C mass ratios, annealed for 12 h at 1000 °C, and vaporized in a modified Krätschmer–Huffman arc reactor under a mixture of ammonia (20 mbar) and helium (200 mbar).

When the rods were packed with 1:1 up to 1:3 ratios of La_2O_3/C, the fullerene yield was very low; however, when the ratio was changed to 1:4, the yield increased (Figure 1). As anticipated, the C_{96} cage is preferentially templated by the La_3N cluster. From the MALDI-TOF mass spectrum, a large carbon cage distribution was observed, with cages as large as C_{104} and as small as C_{86}. These results demonstrate that the synthesis and isolation of large fullerene cages is possible by increasing the size of the metallic cluster encapsulated, and that metallic clusters larger than Ce_3N are preferentially encapsulated inside C_{96} carbon cages.

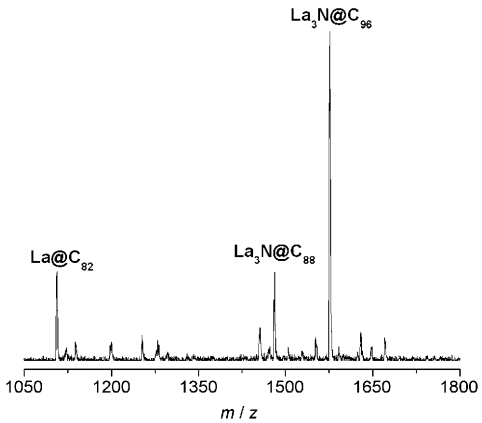

Figure 1. MALDI-TOF mass spectrum of the $La_3N@C_{2n}$ clusterfullerene family using a La_2O_3/C 1:4 ratio.

Even though the mass spectrum showed that $La_3N@C_{2n}$ metallofullerenes are formed during the arcing process, the total fullerene yield still remained low. When the La_2O_3/C ratio was increased to 1:5, a significant increase in fullerene yield was obtained ($\approx$0.1 mg per every five burned rods). Other La_2O_3/C ratios were tried, but in those cases the packed material was unstable, under arcing conditions.

Figure 2 shows the MALDI-TOF mass spectrum and HPLC trace of the $La_3N@C_{2n}$ clusterfullerene family using a 1:5 La_2O_3/C ratio. Note that as this ratio increases from 1:4 to 1:5 the mass distribution changes dramatically, but $La_3N@C_{96}$ still remains as one of the major products. A significant increase in the $La_3N@C_{88}$ yield is also observed. Another noteworthy point is that a wider carbon-cage distribution of $La_3N@C_{2n}$ cluster fullerenes is formed, with cages ranging from C_{86} to C_{110}, making this family of metallofullerenes the largest in terms of cluster and carbon-cage sizes.

The fact that the metallofullerene yield decreases when the size of the metallic cluster increases suggests that the cluster size plays the most important role in terms of carbon-cage distribution, abundance, and preference for a given fullerene template.[14,15] For example, $Sc_3N@C_{2n}$ ($r_{Sc^{3+}} = 0.745$ Å) preferentially templates the C_{80} cage, producing the highest fullerene yield, whereas $Gd_3N@C_{2n}$ ($r_{Gd^{3+}} = 0.938$ Å) continues to prefer the C_{80} cage but produces the lowest yield.

Metallic clusters larger than Gd_3N such as Nd_3N, Pr_3N and Ce_3N are preferentially encapsulated inside a C_{88} cage, and the fullerene yield increases in the order $Ce_3N@C_{2n}$ ($r_{Ce^{3+}} = 1.010$ Å) < $Pr_3N@C_{2n}$ ($r_{Pr^{3+}} = 0.997$ Å) < $Nd_3N@C_{2n}$ ($r_{Nd^{3+}} = 0.983$ Å).[20] Since metallic nitride endohedral fullerenes appear in larger abundance templating the C_{80} rather than the C_{88} cage (with the exception of $Gd_3N@C_{2n}$),

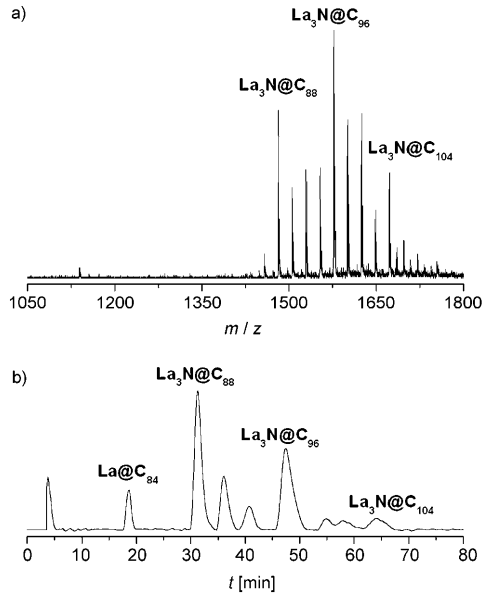

Figure 2. a) Mass spectrum of the $La_3N@C_{2n}$ clusterfullerene family using a La_2O_3/C 1:5 ratio and b) HPLC chromatogram.

it was not surprising to find that $La_3N@C_{2n}$ ($r_{La^{3+}} = 1.045$ Å) produces the lowest fullerene yield among all the metallic nitride endohedral fullerenes under the same preparation conditions. Also, it should be noted that under our arcing conditions, $Eu_3N@C_{2n}$ and $Sm_3N@C_{2n}$ are not formed. As suggested by Gu and co-workers, this is likely due to product yields being associated with thermal properties of the caged metals, such as boiling points.[18] Current work in our group is underway to understand this dependence.

Isolation and purification of the $La_3N@C_{2n}$ endohedral fullerenes: Using our optimized condition, we were only able to isolate and purify $La_3N@C_{88}$, $La_3N@C_{92}$ and $La_3N@C_{96}$. The identity and purity of these three metallofullerenes were established by their HPLC chromatograms, mass spectra and SEM/EDS analysis. The much lower yield of the other fractions prevented their isolation (see Figures 3–6).

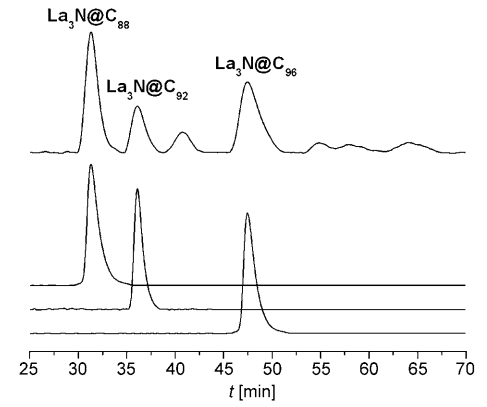

Figure 3. HPLC chromatogram of the $La_3N@C_{2n}$ clusterfullerene family and isolated fractions. Buckyprep-M column; toluene flow rate = 4.00 mL min^{-1}; detection at 372 nm.

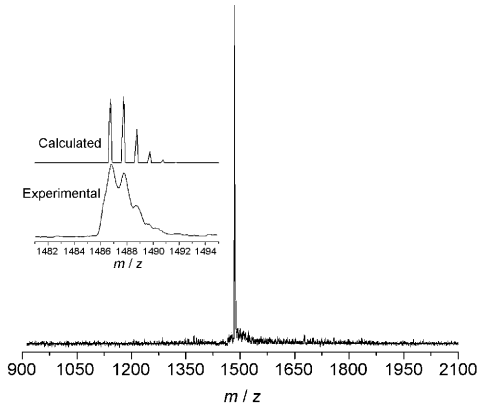

Figure 4. Calculated and experimental mass spectrum of $La_3N@C_{88}$.

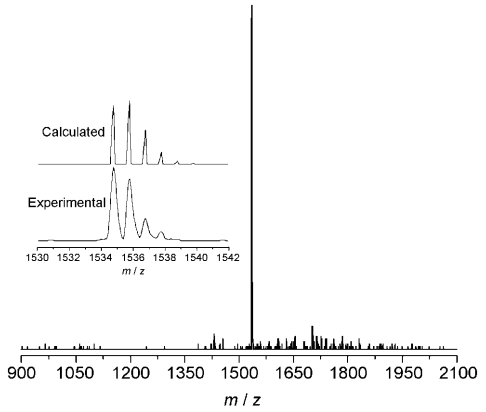

Figure 5. Calculated and experimental mass spectrum of $La_3N@C_{92}$.

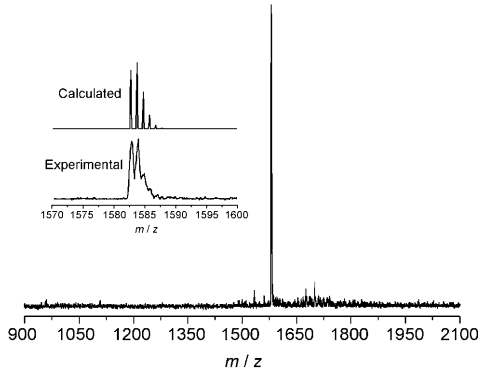

Figure 6. Calculated and experimental mass spectrum of $La_3N@C_{96}$.

Using a semipreparative Buckyprep-M column the three main fractions were isolated in considerably high purity. The purity was checked by HPLC injections using both Buckyprep-M and Buckyprep columns, followed by MALDI-TOF mass analysis in both positive and negative ion modes.

A closer look at the positive ion mode MALDI TOF MS (Figures 4–6) of these metallofullerenes shows an excellent agreement between the calculated and experimental isotopic distributions, confirming their chemical identities. Further-

more, samples of $La_3N@C_{2n}$ ($n=44$, 46 and 48) were deposited on TEM grids and submitted to energy dispersive spectroscopy (EDS) analysis (Figure 7), which showed the characteristic peaks of lanthanum, giving further proof of the nature of these endohedral fullerenes.

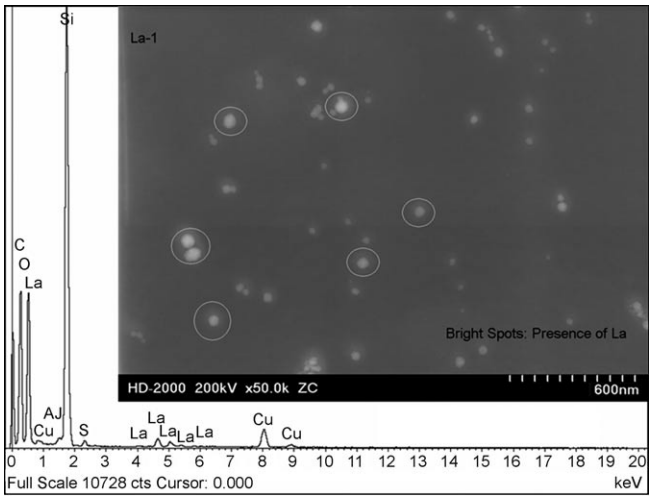

Figure 7. SEM/EDS of $La_3N@C_{88}$. Copper and aluminium come from the grid and sample holder. Sulfur and oxygen probably come from the solvents used to manipulate the samples (ether and carbon disulfide). And Si comes as an impurity after passing the sample through a silica column (in a Pasteur pipette) after electrochemical analysis.

From the HPLC chromatogram and the amounts of metallofullerenes collected, it was observed that $La_3N@C_{96}$ corresponds to 36% of the extracted metallofullerenes while $La_3N@C_{88}$ represents 33%.

It is important to note from the mass spectrum and HPLC chromatogram (Figure 2) that beyond $La_3N@C_{96}$, the yield decreases until $La_3N@C_{104}$, where an appreciable increase is observed. Such a yield distribution suggests that if larger metallic nitride clusters could be formed the expected templated fullerene would be the C_{104} cage. An interesting finding is that the preferentially templated fullerene cages seem to increase in size exactly by eight carbons as the size of the metallic nitride increases. The nature of this stabilization phenomenon remains uncertain and calculations are currently underway in order to understand this discrete increase.

Electrochemical studies of $La_3N@C_{2n}$ endohedral fullerenes: Electrochemical studies were conducted in a solution of 0.05 M NBu_4PF_6 (supporting electrolyte) in *o*-dichlorobenzene (*o*-DCB). A 2 mm diameter glassy carbon disk was used as the working electrode. Ferrocene was added at the end of the experiments as an internal reference for measuring potentials.

The redox properties of metallic nitride endohedral fullerenes ranging from C_{80} to C_{88} cages have shown a progressive decrease of the HOMO–LUMO gaps as the size of the carbon cage increases, and irreversible reductions that become reversible when the carbon cage reaches the C_{88} size.[14–16] However, from C_{88} to C_{96} this straightforward tendency is not observed (Figure 8).

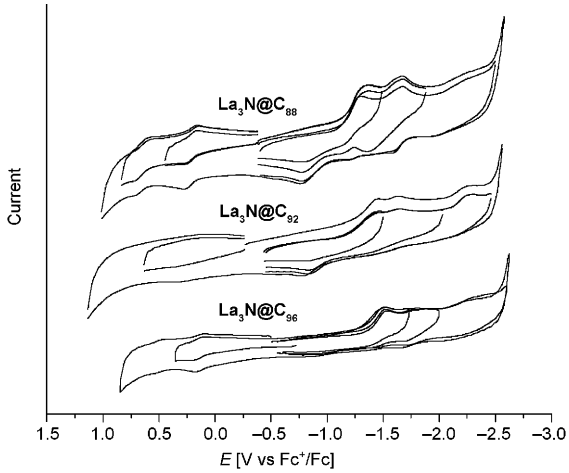

Figure 8. Cyclic voltammograms of $La_3N@C_{88}$, $La_3N@C_{92}$, and $La_3N@C_{96}$ in 0.05 M NBu_4PF_6/*o*-DCB with ferrocene as internal standard. Scan rate = 0.1 V s^{-1}.

$La_3N@C_{2n}$ ($n=44$, 46 and 48) metallofullerenes exhibit three irreversible reduction and two irreversible oxidation steps. Their electrochemical HOMO–LUMO gaps are 1.57, 1.80, and 1.68 V respectively for $La_3N@C_{88}$, $La_3N@C_{92}$ and $La_3N@C_{96}$ (Table 1).

Table 1. Half wave potentials vs Fc^+/Fc of the reduction and oxidation steps of $La_3N@C_{88}$, $La_3N@C_{92}$ and $La_3N@C_{96}$.

TNT EMF[a]	E_p red$_1$	E_p red$_2$	$E_{1/2}$ ox$_1$	$E_{1/2}$ ox$_2$	ΔE_{gap}
$La_3N@C_{88}$	−1.36	−1.67	0.21	0.66	1.57
$La_3N@C_{92}$	−1.44	−1.64	0.36		1.80
$La_3N@C_{96}$	−1.54	−1.77	0.14	0.53	1.68

[a] Trimetallic nitride endohedral metallofullerene.

A very interesting finding is that with the exception of $La_3N@C_{88}$, the electrochemistry of all the $M_3N@C_{88}$ (M = Gd, Nd, Pr and Ce) metallofullerenes studied by our group have shown two reversible oxidations (the first one at very low potentials ≈0.06–0.08 V), a reversible first reduction, a second quasi-reversible reduction and what is likely a multielectronic third reduction step.[14–16] Those metallofullerenes also have very low HOMO–LUMO gaps (≈1.38–1.46 V). Nevertheless, $La_3N@C_{88}$ seems to behave differently (Figure 9 and Table 2), exhibiting two irreversible oxidation and reduction steps. Additionally, it has a slightly larger HOMO–LUMO gap of 1.57 V. Increasing the scan rates (100 mV s^{-1} to 2 V s^{-1}) did not improve the reversibility of the reduction waves.

Due to the low yield of $M_3N@C_{92}$ (M = Pr and Ce) metallofullerenes, we were unable to isolate these for electrochemical studies and to compare to $La_3N@C_{92}$. However,

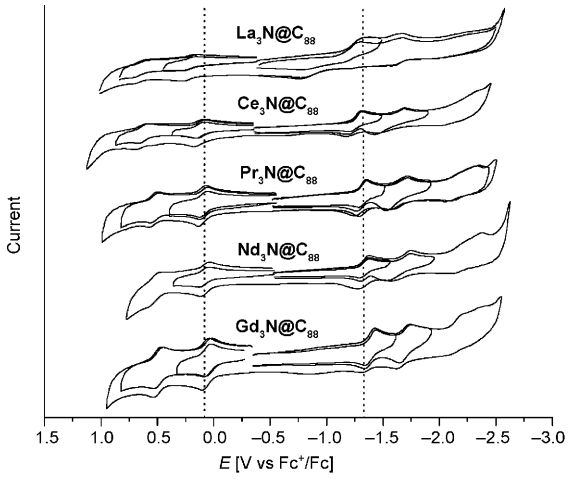

Figure 9. Cyclic voltammograms of $M_3N@C_{88}$ (M = La, Ce, Pr, Nd and Gd) in 0.05 M NBu_4PF_6/*o*-DCB with ferrocene as internal standard. Scan rate = 0.1 V s^{-1}.

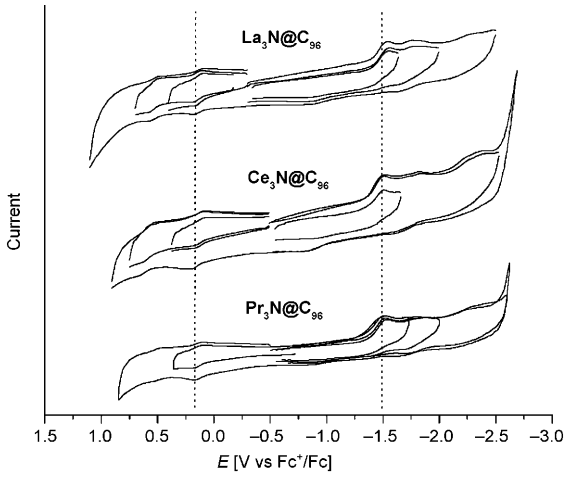

Figure 10. Cyclic voltammograms of $La_3N@C_{96}$, $Ce_3N@C_{96}$ and $Pr_3N@C_{96}$ in 0.05 M NBu_4PF_6/*o*-DCB with ferrocene as internal standard. Scan rate = 0.1 V s^{-1}.

Table 2. Half wave potentials ($E_{1/2}$) or peak potentials (E_p) vs Fc^+/Fc of the reduction and oxidation steps of several $M_3N@C_{88}$ metallofullerenes.

TNT EMF	EN[a]	$E_{1/2}$ red$_1$	$E_{1/2}$ ox$_1$	ΔE_{gap}
$Gd_3N@C_{88}$	1.20	−1.40	0.06	1.46
$Nd_3N@C_{88}$	1.14	−1.33	0.07	1.40
$Pr_3N@C_{88}$	1.13	−1.31	0.09	1.40
$Ce_3N@C_{88}$	1.12	−1.30	0.08	1.38
$La_3N@C_{88}$	1.10	E_p = −1.36	E_p = 0.21	1.57

[a] Pauling electronegativity.[20]

samples of $Pr_3N@C_{96}$ and $Ce_3N@C_{96}$ were synthesized, isolated, and purified as reported earlier.[15]

Figure 10 shows cyclic voltammograms of the $M_3N@C_{96}$ (M = Pr, Ce and La) metallofullerenes. These compounds exhibit similar redox behavior, with two reversible oxidations and two irreversible reductions; a third, possibly multielectronic, irreversible reduction is also observed. Their electrochemical HOMO–LUMO gaps also have similar values (see Table 3).

Table 3. Cathodic peak potential of reduction steps and half wave potentials vs Fc^+/Fc of oxidation steps of $Pr_3N@C_{96}$, $Ce_3N@C_{96}$ and $La_3N@C_{96}$.

TNT EMF	$r(M^{3+})$ [Å^3]	E_p red$_1$	E_p red$_2$	$E_{1/2}$ ox$_1$	$E_{1/2}$ ox$_2$	ΔE_{gap}
$Pr_3N@C_{96}$	0.997	−1.51	−1.86	0.14	0.53	1.65
$Ce_3N@C_{96}$	1.010	−1.50	−1.84	0.18	0.67	1.68
$La_3N@C_{96}$	1.045	−1.54	−1.77	0.14	0.53	1.68

All metallofullerenes of the same cage-size and different metallic nitride cluster have shown similar redox behavior and HOMO–LUMO gaps, suggesting that the carbon cage symmetry is probably the same for each size. $La_3N@C_{88}$ is an exception, which may be an indication that the cage symmetry is different or that due to the cluster size the interactions between the cluster and the carbon cage are stronger for this metallofullerene. X-ray data are necessary to confirm this suggestion.

UV/Vis-NIR studies of $La_3N@C_{2n}$ endohedral fullerenes: UV/Vis-NIR studies have proven to be very useful in metallofullerene research because they give insight about the symmetry of the fullerene cage and their optical HOMO–LUMO gaps, since absorptions of these compounds are mainly due to π–π* transitions.[3,19] Samples of $La_3N@C_{2n}$ (n = 44, 46 and 48) were dissolved in toluene and their UV/Vis-NIR spectra were recorded using a Perkin–Elmer Lambda 950 spectrophotometer. Figure 11 shows the superimposed spectra of the isolated La_3N endohedral fullerene fractions while table 4 lists absorption values and optical onset of these metallofullerenes.

$La_3N@C_{88}$ exhibits absorptions at 395, 479, 602, 768 and 965 nm. Except for the absorption at 602, these values are in the same range as those found for other $M_3N@C_{88}$ (M = Nd,

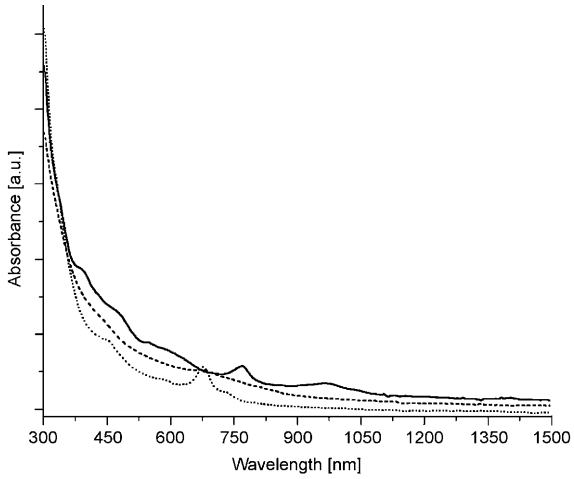

Figure 11. UV/Vis-NIR spectra of $La_3N@C_{88}$ (——), $La_3N@C_{92}$ (-----), and $La_3N@C_{96}$ (•••••) dissolved in toluene.

Pr and Ce) metallofullerenes.[15] However, the spectral onset of $La_3N@C_{88}$ is located around 1330 nm, which results in an optical gap $\approx$0.93 V higher than the optical gaps reported for the same cage-size counterparts, in agreement with the electrochemical band gaps for all these metallofullerenes.

Unlike what was observed by electrochemistry, where the electrochemical gaps differed significantly, the optical gaps of $La_3N@C_{92}$ and $La_3N@C_{96}$ exhibit similar values (1.08 and 1.09 V, respectively) with absorptions exclusively in the UV/Vis region (see Table 4).

Table 4. Characteristic UV/Vis-NIR absorptions and absorption onset of some $La_3N@C_{2n}$ ($n=44$, 46, and 48).

TNT EMF	Onset [nm]	Band gap [eV][a]	UV/Vis-NIR absorptions peaks [nm]
$La_3N@C_{88}$	1330	0.93	395, 479, 602, 768, 965
$La_3N@C_{92}$	1147	1.08	342, 449, 674
$La_3N@C_{96}$	1136	1.09	450, 583, 677, 733

[a] Band-gap calculated from the spectral onset (bandgap (eV) $\approx$1240/onset (nm)[11]).

Conclusion

The $La_3N@C_{2n}$ ($43 \leq n \leq 55$) endohedral metallofullerene family was successfully synthesized for the first time by arcing packed rods in a modified Krätschmer-Huffman arc reactor. From the raw soot, La_3N cluster endohedral fullerenes were extracted, isolated and purified. Three main fractions were characterized by MALDI-TOF mass spectroscopy, SEM/EDS analysis, UV/Vis-NIR, and cyclic voltammetry. La_3N represents the largest metallic nitride cluster encapsulated to date inside fullerene cages, with preference for the C_{96} cage. This represents the first example of this cage being preferentially formed. The electrochemical properties of this family showed that $La_3N@C_{88}$ exhibits irreversible oxidation and reduction steps, unlike other $M_3N@C_{88}$ metallofullerenes. In general $La_3N@C_{92}$ and $La_3N@C_{96}$ present similar electrochemistry, UV/Vis-NIR absorptions and HOMO–LUMO gaps.

Experimental Section

High purity graphite rods (6 mm diameter), purchased from POCO, were core-drilled (4 mm diameter) and packed with different mass ratios of graphite powder and La_2O_3 (lanthanum oxide). The rods were annealed at 1000 °C for 12 h and then vaporized in a Krätschmer–Huffman arc reactor under a mixture of ammonia (20 mbar) and helium (200 mbar) using an arc current of 85 A. The soot collected from the arc reactor for each packed rod was extracted with CS_2 in a sonicator for about two hours. After removal of the solvent, the crude mixtures were washed with ether and acetone until the solution was no longer colored. The solids were dissolved in toluene, filtered and separated by HPLC using a semipreparative 10 mm × 250 mm Buckyprep-M column with a flow rate of 4.00 mL of toluene per minute. Isolated samples were then passed through a linear combination of Buckyprep and Buckyprep-M columns with a flow rate of 2.00 mL of toluene per minute without any further sign of isomeric separation. Preparation of $Pr_3N@C_{96}$ and $Ce_3N@C_{96}$ is reported elsewhere.[15] MALDI-TOF mass spectrometry was carried out using a Bruker Omni Flex. Cyclic voltammetry was carried out in a one-compartment cell connected to a BAS 100B workstation in a solution of *o*-DCB containing 0.05 M NBu_4PF_6. A 2 mm diameter glassy carbon disk was used as the working electrode. Ferrocene was added to the solution at the end of each experiment as internal standard, and all the electrochemical potentials were referenced to its redox couple. After CV, the samples were passed through a silica column (Pasteur pipette) for removal of the electrolyte and ferrocene. For the EDS analysis, the samples were deposited on TEM grids and the spectra were taken on a HD-2000 STEM, equipped with an Oxford EDS system. UV/Vis-NIR spectra were taken using a Perkin-Elmer Lambda 950 spectrophotometer.

Acknowledgements

Financial support from the National Science Foundation to A.J.A. and L.E. (Grant number CHE-0509989) is greatly appreciated. This material is based on work supported by the National Science Foundation while L.E. was working there. All opinions, findings, conclusions, or recommendations expressed herein are those of the authors and do not necessarily reflect the views of the National Science Foundation. The authors also gratefully thank Greg Becht and Prof. Shiou-Jyh Hwu for their help in the annealing of the composite rods.

[1] S. Stevenson, G. Rice, T. Glass, K. Harich, F. Cromer, M. R. Jordan, J. Craft, E. Hajdu, R. Bible, M. M. Olmstead, K. Maitra, A. J. Fisher, A. L. Balch, H. C. Dorn, *Nature* **1999**, *401*, 55–57.
[2] J. M. Campanera, C. Bo, J. M. Poblet, *Angew. Chem.* **2005**, *117*, 7396–7399; *Angew. Chem. Int. Ed.* **2005**, *44*, 7230–7233.
[3] L. Dunsch, M. Krause, J. Noack, P. Georgi, *J. Phys. Chem. Solids* **2004**, *65*, 309.
[4] M. Mikawa, H. Kato, M. Okumura, M. Narataki, Y. Kanazawa, N. Miwa, H. Shinohara, *Bioconjugate Chem.* **2001**, *12*, 510–514.
[5] H. Kato, Y. Kanazawa, M. Okumura, A. Taninaka, T. Yokawa, H. Shinohara, *J. Am. Chem. Soc.* **2003**, *125*, 4391–4397.
[6] S. Stevenson, H. M. Lee, M. M. Olmstead, C. Kozikowski, P. Stevenson, A. L. Balch, *Chem. Eur. J.* **2002**, *8*, 4528.
[7] M. Krause, J. Wong, L. Dunsch, *Chem. Eur. J.* **2005**, *11*, 706–711.
[8] S. Stevenson, J. P. Phillips, J. E. Reid, M. M. Olmstead, S. P. Rath, A. L. Balch, *Chem. Commun.* **2004**, 2814–2815.
[9] M. Krause, L. Dunsch, *Angew. Chem.* **2005**, *117*, 1581–1584; *Angew. Chem. Int. Ed.* **2005**, *44*, 1557–1560.
[10] M. Wolf, K.-H. Müller, Y. Skourski, D. Eckert, P. Georgi, M. Krause, L. Dunsch, *Angew. Chem.* **2005**, *117*, 3371–3374; *Angew. Chem. Int. Ed.* **2005**, *44*, 3306–3309.
[11] S. Yang, L. Dunsch, *J. Phys. Chem. B* **2005**, *109*, 12320–12328.
[12] T. Zuo, C. M. Beavers, J. C. Duchamp, A. Campbell, H. C. Dorn, M. M. Olmstead, A. L. Balch, *J. Am. Chem. Soc.* **2007**, *129*, 2035–2043.
[13] a) S. Stevenson, P. W. Fowler, T. Heine, J. C. Duchamp, G. Rice, T. Glass, K. Harich, E. Hajdu, R. Bible, H. C. Dorn, *Nature* **2000**, *408*, 427; b) M. M. Olmstead, A. de Bettencourt-Dias, J. C. Duchamp, S. Stevenson, H. C. Dorn, A. L. Balch, *J. Am. Chem. Soc.* **2000**, *122*, 12220–12226; c) S. Yang, M. Kalbac, A. Popov, L. Dunsch, Lothar, *ChemPhysChem* **2006**, *7*, 1990–1995; d) S. Yang, A. A. Popov, L. Dunsch, *J. Phys. Chem. B* **2007**, *111*, 13659–13663; e) N. Chen, E. Zhang, C. Wang, *J. Phys. Chem. B* **2006**, *110*, 13322–13325; f) X. Wang, T. Zuo, M. M. Olmstead, J. C. Duchamp, T. E. Glass, F. Cromer, A. L. Balch, H. C. Dorn, *J. Am. Chem. Soc.* **2006**, *128*, 8884–8889; g) N. Chen, L. Fan, K. Tai, Y, Wu, C. Shu, X. Lu, C. Wang, *J. Phys. Chem. C* **2007**, *111*, 11823–11828.
[14] F. Melin, M. N. Chaur, S. Engmann, B. Elliott, A. Kumbhar, A. J. Athans, L. Echegoyen, *Angew. Chem.* **2007**, *119*, 9190–9193; *Angew. Chem. Int. Ed.* **2007**, *46*, 9032–9035.
[15] M. N. Chaur, F. Melin, B. Elliott, A. Kumbhar, A. J. Athans, L. Echegoyen, *Chem. Eur. J.* **2008**, *14*, 4594–4599.

[16] M. N. Chaur, F. Melin, B. Elliott, A. J. Athans, K. Walker, B. C. Holloway, L. Echegoyen, *J. Am. Chem. Soc.* **2007**, *129*, 14826–14829.
[17] C. M. Cardona, B. Elliott, L. Echegoyen, *J. Am. Chem. Soc.* **2006**, *128*, 6480–6485.
[18] Y. Lian, Z. Shi, X. Zhou, X. He, Z. Gu, *Chem. Mater.* **2001**, *13*, 39–42.
[19] H. Shinohara, *Rep. Prog. Phys.* **2000**, *63*, 843–892.
[20] *CRC Handbook of Chemistry and Physics*, 81st ed. (Ed.: D. R. Lide), CRC Press, New York City, **2000**.

Received: May 8, 2008
Published online: July 28, 2008

